A study of direct forging process for powder superalloys

Bai, Q.; Lin, J.; Jiang, J.; Dean, Trevor; Zou, J.; Tian, G.

DOI:
10.1016/j.msea.2014.10.039

Materials Science & Engineering A 621 (2015) 68–75

Contents lists available at ScienceDirect

Materials Science & Engineering A

journal homepage: www.elsevier.com/locate/msea

A study of direct forging process for powder superalloys

Q. Bai [a], J. Lin [a,*], J. Jiang [a], T.A. Dean [b], J. Zou [c], G. Tian [c]

[a] Department of Mechanical Engineering, Imperial College London, London SW7 2AZ, UK
[b] Departments of Mechanical Engineering, University of Birmingham, Birmingham B15 2TT, UK
[c] Beijing Institute of Aeronautical Materials, Beijing 100095, China

ARTICLE INFO

Article history:
Received 22 July 2014
Received in revised form
15 October 2014
Accepted 16 October 2014
Available online 24 October 2014

Keywords:
Direct powder forging
Nickel based superalloys
Powder densification
Microstructural evolution
Microhardness evolution
FEM of powder forging densification

ABSTRACT

Powder metallurgy (PM) processing of nickel-based superalloys has been used for a wide range of near net-shape fine grained products. In this paper a novel forming process, i.e. direct forging of unconsolidated powder superalloys is proposed. In this process, encapsulated and vacuumed powder particles are heated up to a forming temperature and forged directly at high speed to the final shape, by using a high forming load. Experiments of direct powder forging have been conducted on an upsetting tool-set. Microstructure, relative density and hardness of the formed specimen have been investigated. A finite element model of the direct powder forging process has been established in DEFORM and validated by the comparisons of experimental with simulation results of load variation with stroke as well as relative density distribution. The stress state and the relative density variation have been obtained from FE simulation. The correlation between the stress and consolidation condition has been rationalised. The developed FE model can provide a guide to design the geometry and thickness of preform for direct powder forging.

1. Introduction

Powder superalloys have been widely used to produce high performance components [1]. Four typical powder metallurgy methods for superalloys are hot isostatic pressing [2], hot isostatic pressing+hot isothermal forging [3,4], hot isostatic pressing or hot unidirectional pressing+hot extrusion+hot isothermal forging [5]. Hot isostatic pressing (HIPing), as an important near net-shape forming process, allows dense, precisely-shaped components to be formed from metal powders. However, HIPing is extremely costly. During a HIPing process, the powder, which is packed into an evacuated sheet metal preform container, is degassed and sealed under vacuum, and then the container with powder is heated and simultaneously subjected to a gas pressure (usually argon) in a pressure vessel for a long time [6,7], resulting in high cost and low productivity. Furthermore, an intrinsic problem is that prior particle boundary (PPB) precipitate networks can occur in the HIPing process [8]. PPB precipitation has been the major issue that largely limits the application of net-shaped HIPing to nickel-based superalloys. It is generally believed that PPBs are caused by particle contamination and atomic segregation during the long heating time. Both result in precipitation at PPBs, either as carbides, oxides, oxy-carbides, or possibly as oxy-carbonitrides [9]. Since PPB precipitates are brittle and thus provide an easy fracture path, the undesirable PPB networks are detrimental to mechanical properties of HIPed nickel alloy components. In order to break up the PPB networks and restore mechanical properties, post-HIPing deformation, e.g. hot extrusion and hot isothermal forging, is needed, which increases cost.

With regard to powders of other metal alloys, sintered powder forging of steel now is widely used commercially to produce load bearing components, particularly in drive trains of automobiles [10]. Some studies have been carried out on aluminium powder forging [11–13]. Dashwood and Schaffer [11] carried out a hot forging test on a sintered specimen of aluminium alloy and found that the porosity was effectively removed due to compression strain. However due to the fragility of nickel-based superalloy green compacts, it is difficult to use sinter-forge technology for them. In order to reduce the oxidation during heating and soaking of the powder, Das et al. [14] poured Fe–P powder into an cylinder metal container with two open ends, used dry hydrogen flowing through to remove the oxide layer from the powder surface, and heated the powder and the container in a furnace simultaneously. The powder was then hot forged to achieve the final shape. However the best relative density they could obtain was 0.976 in the forged slabs, which may be due to the trapped hydrogen gas between the powders. Using a degassed and sealed metal container can reduce the gas trapped between powders as well as prevent powders from oxidation.

With regard to superalloy compaction techniques, Kelsey Hayes ROC developed a rapid omnidirectional compaction (i.e. fluid die process) in 1979 [15], which does not require a costly HIPing unit for consolidation. In this method, recyclable 'fluid' dies consisting

* Corresponding author. Tel.: +44 20 7594 7082.
E-mail address: jianguo.lin@imperial.ac.uk (J. Lin).

http://dx.doi.org/10.1016/j.msea.2014.10.039

of a nickel-copper alloy have been used. At high temperature, the die softens and pressure applied to the die is transmitted to the powder. However the geometry of the 'fluid' die cavity is changed after hot compaction due to the shrinkage of the superalloy powder and therefore it is necessary to produce another die each time after deformation. Crucible Industries developed ceramic mould for HIPing process in 1987 [16], in which superalloy powder is filled into a porous ceramic container. The ceramic container is inserted into a larger steel container which is subsequently filled with a pressure-transmitting bed of fine Al_2O_3 powder, and degased and sealed. In the HIPing process, the steel container is subject to a gas pressure, and the pressure is then transmitted to the ceramic container via Al_2O_3 powder to obtain extremely complex shapes. However HIPing process results in high cost and low productivity. Meeks and Fleming [17] developed a ceramic consolidation (Ceracon) process, which involves taking a heated preform and consolidating the material by pressure against a granular ceramic medium using a conventional forging press [18].

Many researchers have been working on the relationship between pressure and time to process completion, during HIPing [19–21]. Arzt and Ashby [7] studied the effect of pressure and time on relative density for superalloys. As shown in Fig. 1(a), they found that the deformation mechanisms changed from diffusion at a low-pressure to power-law creep at an intermediate pressure and then to yield at a high-pressure. As HIPing pressure is increased, less time is needed to achieve full density of the powder. Based on their research, a diagram was generated as shown in Fig. 1(b). The symbols indicate the relationship between pressure and time when the relative density reaches 1.0, which are obtained from Fig. 1(a). Therefore if the pressure is increased, the time for obtaining a fully dense material could be reduced following a logarithmic form.

In this paper a novel forming process, i.e. direct powder forging of powdered nickel-based superalloys is proposed. In this process, the encapsulated and vacuumed powder is heated up to a forming temperature and forged directly to the final shape, by using a high forming load for a very short time. Direct powder forging is a low-cost and energy-saving process compared to conventional PM processes. Also readily available conventional forging press machines can be used for direct powder forging. A shorter heating time results in fewer PPB precipitates, and due to a large amount of plastic deformation, the existing PPB networks are broken up and thus the detrimental effect of PPBs is weakened. In this paper an up-setting test was conducted to investigate the direct powder forging process. Microstructure, relative density and hardness have been investigated. A finite element model of direct powder forging has been developed in DEFORM-3D.

2. Experimental setup and method

Argon atomised superalloy FGH96 powder, supplied by Beijing Institute of Aeronautical Materials (BIAM), was used as the starting powder. Its chemical composition is given in Table 1. Laser diffraction particle size analyser Malvern Mastersizer 2000 was used to measure the size of the powder. The size of powder particles followed a standard normal distribution, and the average size was 35 μm based on a number distribution. The gamma prime solvus of this alloy is around 1120 °C.

Due to its good weldability and high stiffness and strength at room temperature and its high ductility at elevated temperature, stainless steel is normally chosen as a container, which is strong enough to maintain shape and dimensional control but soft and malleable at the forming temperature [22]. In this study, powder particles were poured into a cylinder container of stainless steel 304, and then the container was vacuumed to 1.0×10^{-5} Pa in order to reduce the amount of air and thus reduce the oxidation of powder at high temperature. The dimension of the container is shown in Fig. 2(a). The outer diameter of the stainless steel container was 20 mm, the thickness was 2.0 mm and the outer height was 20 mm. The container was coated with glass lubricant to reduce friction during hot forging, as shown in Fig. 2(b).

Upsetting can generate a complex 3-D stress distribution due to contact friction between the test-piece and the tools. In order to study the effect of stress on consolidation in the powder forging process, upsetting test was adopted. The test setup is shown in Fig. 2(c). Two flat dies were mounted on a pillar toolset mounted on a 250 kN ESH single shot high rate testing machine. This high

Table 1
Chemical composition of the FGH96 nickel-based superalloy (wt%) [1].

Cr	Co	Mo	W	Ti	Al	Nb	Zr	C	B	Ni
16	13	4	4	3.7	2.2	0.8	0.036	0.03	0.011	Balance

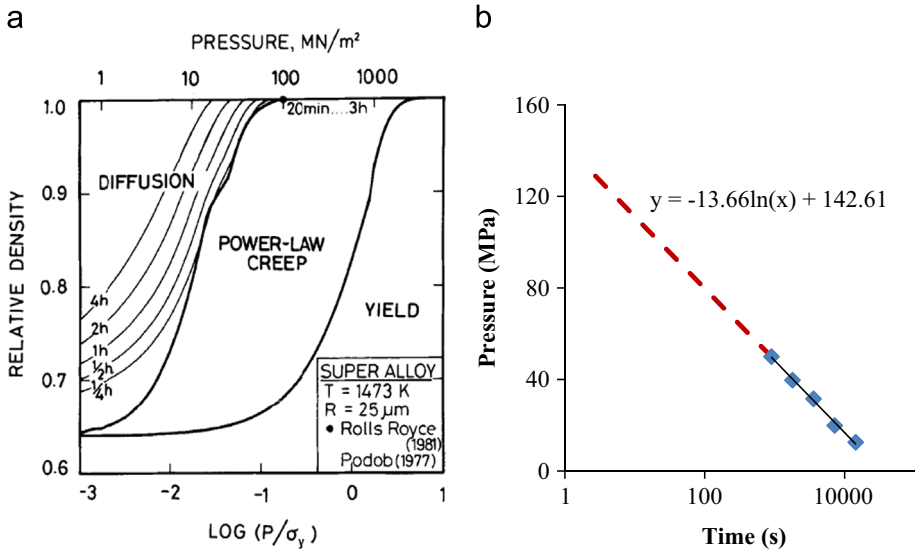

Fig. 1. Concept of direct powder forging: (a) a density/pressure map at $T=1200$ °C for a superalloy with a particle diameter of 50 μm. [7]; (b) relationship between time and pressure for diffusion bonding, at a certain temperature.

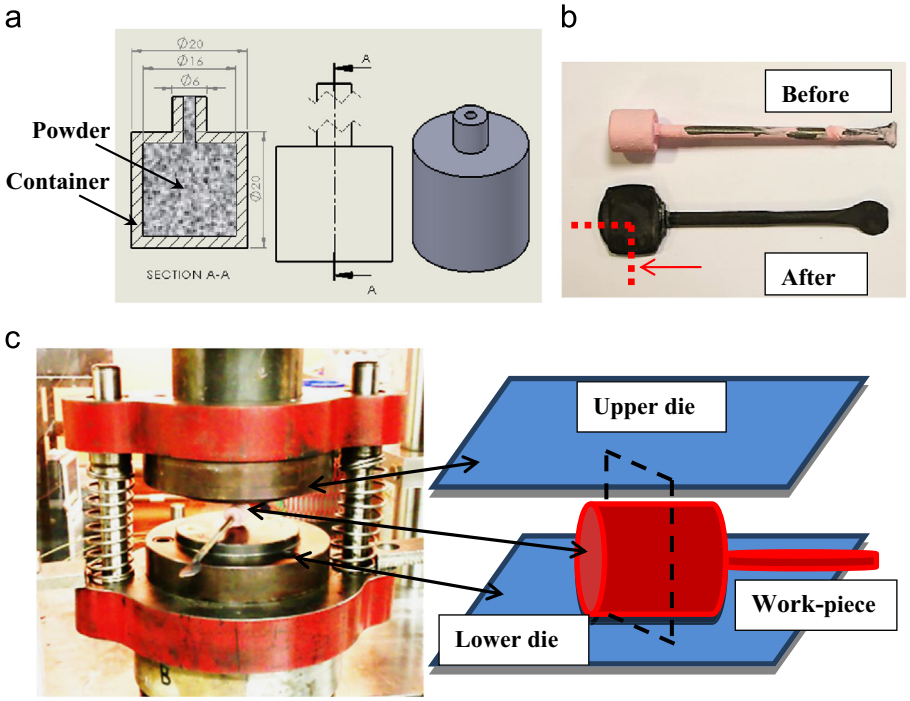

Fig. 2. Test-piece design and test set-up for direct powder forging (a) dimensions of the container; (b) test-piece before and after the deformation; (c) test set-up.

rate servo-hydraulic machine was connected to an oscilloscope to record load and stroke during the forging process. The test-piece, i.e. powder and container, was heated up to 1150 °C (i.e. carbide supersolvus temperature [23]) in a furnace and was soaked for 20 min to obtain thermal equilibrium. Then the test-piece was transferred to the tool-set and was compressed at a speed of 200 mm/s to a final thick sheet shape with a thickness of 5.5 mm. Fig. 2(b) shows the test-pieces before and after the deformation.

In order to study the powder microstructure, a formed test-piece was cut along the red broken lines as shown in Fig. 2(b). The sample was mounted, and the cross section shown by the arrow in Fig. 2(b) was polished and etched in Kalling's solution of 5 g $CuCl_2$, 100 ml of HCl and 100 ml of ethanol [24]. A Hitachi S-3400N scanning electronic microscope (SEM) was used to investigate powder consolidation and microstructure at different locations. Five images were taken at each location. The level of porosity was measured with image analysis software by counting the pixels for the porosity to give the percentage area, and relative density equals 1.0 minus the porosity. An average of the porosity was obtained from the five images at each location. Micro-hardness tests were carried out in the Zwick/Roell hardness testing system at different locations with a load of 50 N, in order to investigate the relationship of relative density and hardness of the material.

3. Experimental results

Since the forging test conducted in this paper is upsetting, the stress is at a maximum in the centre area, which is beneficial to powder consolidation; but due to friction, the stress is much lower in the barrelling area. Fig. 3 shows the microstructure processed by image analysis software Image J at different distances from the centre line. As shown in Fig. 3(a) and (b), within a distance of 7.5 mm from the vertical central line, the powder in this area is almost fully consolidated. The grain size is less than 10 μm, which indicates recrystallisation had occurred. The PPB networks are broken up, and the PPB precipitate distribution is isolated and dispersed in this area. Fig. 3(b) shows a micrograph with a higher magnification. It can be seen that the particles were bonded, no obvious micro-void can be found in this area. At location c, a distance of 10 mm from the vertical centre line, voids can be found as shown by the arrows in Fig. 4(c), and the fraction of voids is less than 5% of the whole area. Recrystallisation (RX) can be found due to severe plastic deformation. However, at location d, the edge of the sample, few powder particles are consolidated since particles in this area were subject to very low stress due to the free end at the barrelling area. The particles are packed relatively loosely, and recrystallisation is difficult to find inside the particles in Fig. 3(d). In the vertical direction at the centre line, as shown in Fig. 3(e) and (f), the powder is fully consolidated, and recrystallisation can be found.

This study focused on the feasibility of this direct powder forging to consolidate powder particles. The demanding microstructure can be obtained by subsequent heat treatment, to control the amount and the size of strengthening phase gamma prime.

Fig. 4 shows the distribution of hardness and relative density with the distance from the centre of the test-piece. The relative density reaches 1.0 within a distance of 7.5 mm from the centre line. It reduces gradually with the increasing distance from 7.5 mm to 10 mm, and then decreases greatly to 0.75 when the distance is larger than 10 mm. The Vickers hardness has a similar trend at different locations. The maximum hardness is found in the centre, with a value of 450 HV. The minimum hardness is at the edge, with a value of 200 HV. The large difference indicates that relative density has a great effect on material hardness: when the relative density decreases from 1.0 to 0.75, the value of hardness decreases almost 50%. This may also be due to lack of particles bonding, as can be seen in Fig. 3(d).

4. Development of the FE model

4.1. Material model

In a HIPing process, it is well documented that three main classes of mechanism dominate: plastic deformation, power-law creep and diffusion densification [6,7]. Atkinson and Davies [25]

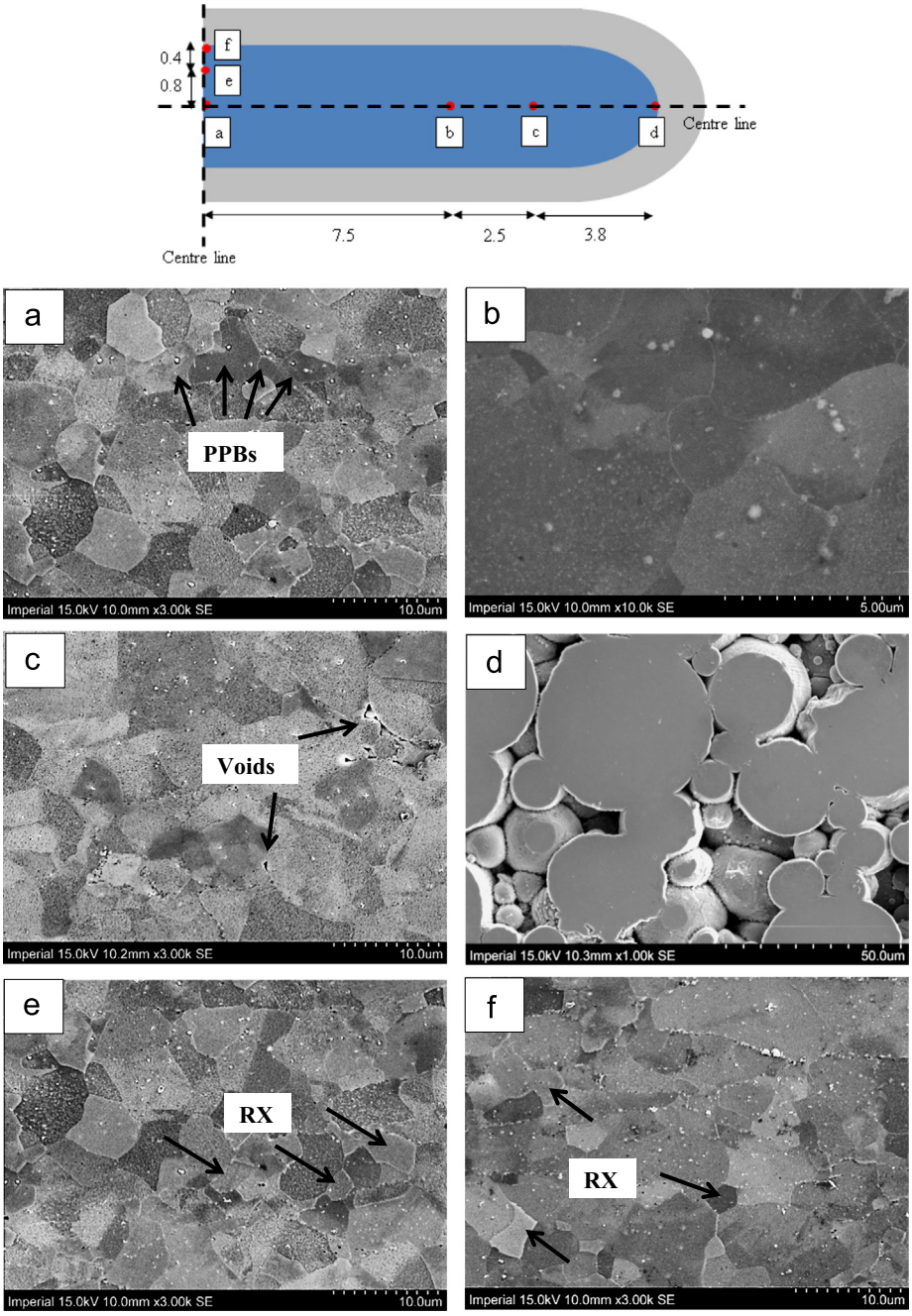

Fig. 3. SEM microstructure observation: typical microstructure at different locations (soaking temperature 1150 °C, soaking time 20 min, and forming speed 200 mm/s).

summarised two different types of material models to describe the thermo-mechanical behaviour of powder in a HIPing process: microscopic and macroscopic models. In microscopic modelling, the various mechanisms of densification, i.e. power-law creep, diffusion etc., are analysed in terms of a single particle and its surroundings. In macroscopic modelling the powder compact is treated as a continuous medium and the constitutive equations which can describe the macroscale deformation of porous materials are obtained by modification of plastic theory for solid materials. Many researchers such as Olevsky [26] and Abouaf [27] used macroscopic modelling to simulate HIPing processes. However, in the powder forging process, due to the high deformation speed and short forming time, plastic deformation dominates the process. In this paper, macroscopic approach is used, and porous material property is defined for the packed powder in finite element software DEFORM. The Shima and Oyane yield surface [28] is used to describe the densification model in the DEFORM porous material model, which reveals that the material density increases with forming deformation, represented by [29]:

$$f(\sigma_{ij}) = AJ_2' + BI_1^2 = Y_R^2 \tag{1}$$

$$A = \frac{3}{1+1/(9f^2)}, \quad f = \frac{0.4}{\sqrt{1-D_R}} \tag{2}$$

$$B = 1/(1+9f^2) \tag{3}$$

where A and B are functions of relative density D_R and Y_R is the yield stress and the porous material in uniaxial compression. J_2' and I_1 are stress invariants. The yield stress of the porous material is related to the yield stress of the fully dense material through the relationship

$$Y_R^2 = \eta Y_b^2 \tag{4}$$

where η is a function of the relative density and Y_b is the yield stress of the fully dense material. Due to the powder particles moving and rotating against each other with interfacial friction, there are differences between a metal powder and a porous material. However with a relative density of 0.7 or greater, the formulations of porous material in DEFORM are appropriate for powder forming [30].

In order to obtain stress–strain curves of FGH96 powder at forming temperatures and strain rates, ideally it is necessary to conduct a uniaxial compression test on the single particle using nano-indentation, but in the present situation this technique is not available at a temperature over 900 °C. Therefore a compression specimen, with a length of 12.0 mm and a diameter of 8.0 mm, from fully dense HIPed material was used, which can be used to approximate the material properties of FGH96 single powder. Since the stainless steel container is deformed in the forging process as well, high temperature uniaxial compression tests were conducted for stainless steel and FGH96. Tests at temperatures of 900 °C, 1000 °C and 1150 °C and strain rates of 0.1 s^{-1}, 1.0 s^{-1} and 10.0 s^{-1} were performed using the computer-controlled thermo-mechanical simulator Gleeble 3800.

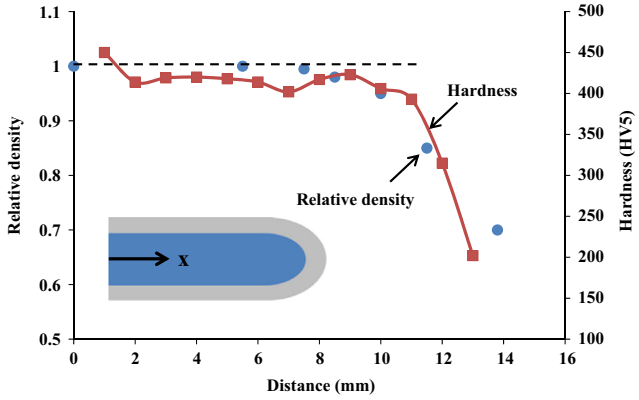

Fig. 4. Distribution of HV5 hardness (solid line with symbols) and relative density (symbols) with the distance from the centre of the test-piece.

Table 2
Temperature dependent parameters.

$k = k_0 \exp\left(\frac{Q_k}{RT}\right)$	$K = K_0 \exp\left(\frac{Q}{RT}\right)$	$C = C_0 \exp\left(-\frac{Q_C}{RT}\right)$
$N = N_0 \exp\left(\frac{Q_n}{RT}\right)$	$E = E_0 \exp\left(\frac{Q_E}{RT}\right)$	

With regard to material constitutive modelling, dislocation-based hardening constitutive equations have been developed by Lin and Liu [31], in which the recovery of dislocations due to annealing and recrystallisation was included for hot forming of boron steel. Also, Li et al. [32], developed a set of unified visco-plastic constitutive equations for boron steel in which damage was considered. In this paper softening mechanisms and recrystallisation are ignored to simplify the constitutive model. The constitutive equations are shown as Eqs. (5)–(8) below:

$$\dot{\varepsilon}^p = \left(\frac{\sigma - H - k}{K}\right)_+^n \tag{5}$$

$$\sigma = E\left(\varepsilon^T - \varepsilon^p\right) \tag{6}$$

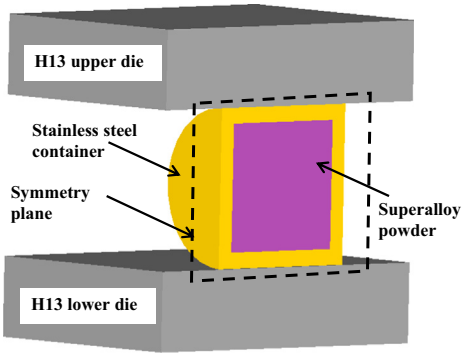

Fig. 5. FE model for direct powder forging process.

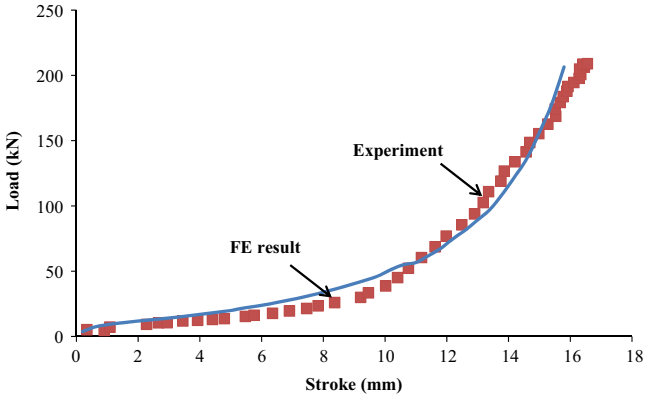

Fig. 6. Comparison of experimental (symbols) and FE (solid line) results for load variation with stroke during powder forging process.

Table 3
Material constants in viscoplastic constitutive equations for stainless steel.

k_0 (MPa)	Q_k (J/mol)	K_0 (MPa)	Q (J/mol)	C_0 (dimensionless)	Q_C (J/mol)	N_0 (MPa)
6.40×10^{-2}	6.43×10^4	1.80	4.0×10^4	1.23×10^4	4.69×10^4	1.71
Q_n(J/mol)	E_0 (dimensionless)	Q_E (J/mol)	M (dimensionless)	n (dimensionless)	γ_1 (dimensionless)	γ_2 (dimensionless)
4.31×10^4	3.61×10^3	8.38×10^3	5.5	5.5	1.2	10

Table 4
Material constants in viscoplastic constitutive equations for FGH96.

k_0 (MPa)	Q_k (J/mol)	K_0 (MPa)	Q (J/mol)	C_0 (dimensionless)	Q_C (J/mol)	N_0 (MPa)
2.76×10^{-16}	4.35×10^5	1.19	5.85×10^4	2.44×10^4	2.65×10^4	1.07×10^{-3}
Q_n (J/mol)	E_0 (dimensionless)	Q_E (J/mol)	M (dimensionless)	n (dimensionless)	γ_1 (dimensionless)	γ_2 (dimensionless)
1.51×10^5	7.59×10^4	5.70×10^3	28	20	0.6	2

$$H = N \cdot \overline{\rho}^{0.5} \tag{7}$$

$$\dot{\overline{\rho}} = M \cdot (1-\overline{\rho}) \cdot \left|\dot{\varepsilon}^{p}\right|^{\gamma_1} - C \cdot \overline{\rho}^{\gamma_2} \tag{8}$$

where ε^T and ε^p are total and plastic strain respectively. Eq. (5) describes the visco-plastic material flow by power law. H is internal stress due to isotropic hardening, and k is the initial yield stress. Eq. (6) is based on Hooke's law. σ is flow stress, and E is the Young's modulus of the material. The material hardening (Eq. (7)) H is calculated according to the accumulation of dislocation density. Eq. (8) calculates normalised dislocation density. The first term of Eq. (8) represents the dislocation accumulation due to plastic deformation and the second term is related to the static recovery of dislocation at hot forming conditions. The constants k, K, B, C, and E, are temperature-dependent parameters and can be formulated by the Arrhenius equation as shown in Table 2. A, n, γ_1 and γ_2 are material constants. The determined material constants for stainless steel and FGH96 are listed in Tables 3 and 4.

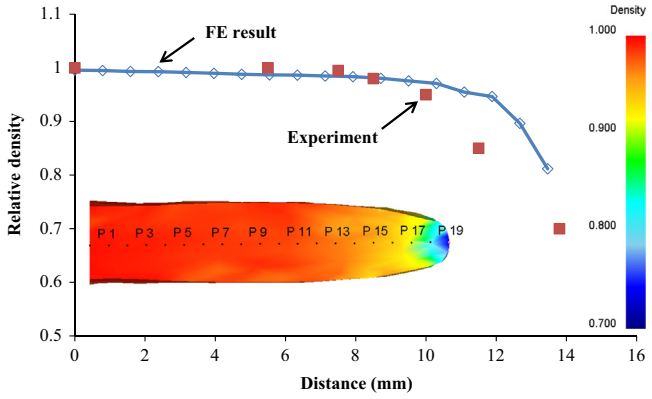

Fig. 7. Comparison of experimental (symbols) and FE (solid line with symbols) results for relative density distribution.

4.2. FE model for direct powder forging process

Simulation of direct powder forging process was carried out using the commercial finite element code DEFORM-3D. The three dimensional finite element model is shown in Fig. 5. Due to symmetry, only half of the test-piece was modelled in the simulation for simplicity and quick calculation. The plane of symmetry is shown in Fig. 5. The initial temperature of the test-piece (i.e. the container and the powder) was 1150 °C, and the initial temperature of the dies was 20 °C. The velocity of the upper die was defined as 100 mm/s since the FE model is symmetric.

In the FE model, the dimensions of the test-piece are the same as those used for the practical tests. Tetrahedral elements were used for container and powder. An initial relative density of 0.7 was defined to the powder as a continuum. The unified visco-plastic constitutve equations were integrated in DEFORM via a user defined subroutine. For the thermal analysis, the thermal properties for stainless steel published by Bogaard et al. [33] were used; for FGH96, the thermal

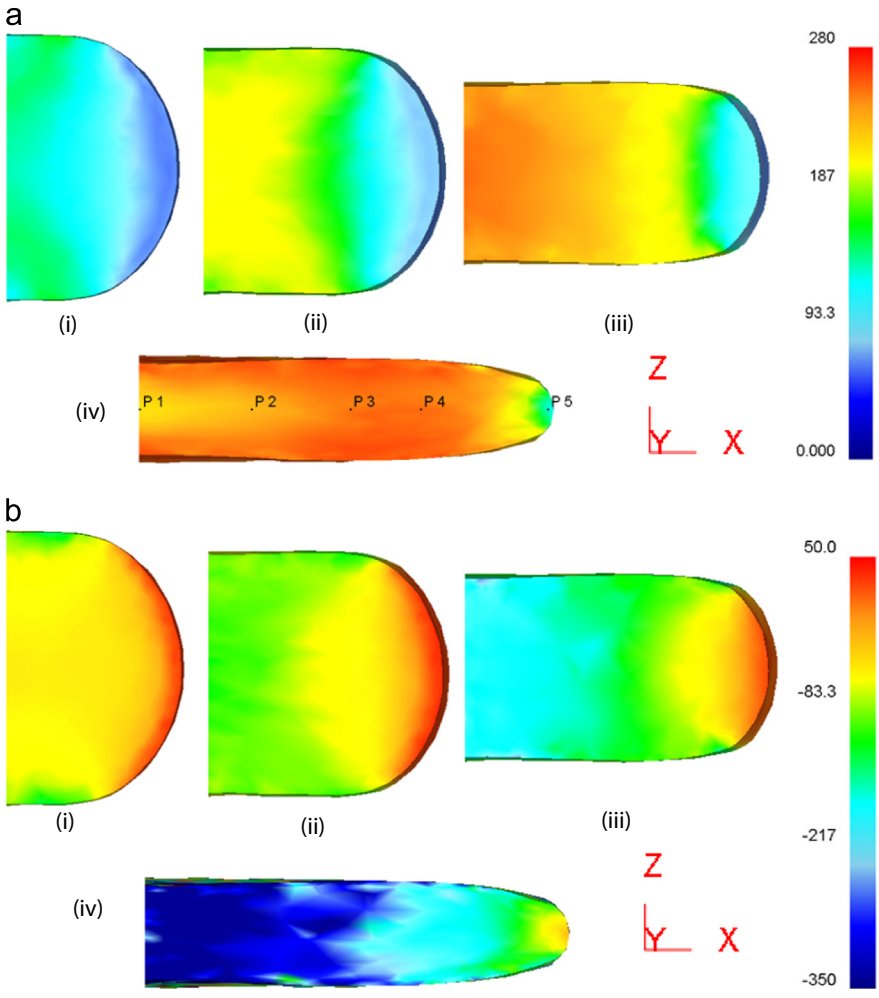

Fig. 8. Distribution of effective stress (MPa) (a) and mean stress (MPa) (b) at different times (MPa). t/t_f is (i) 25%, (ii) 50%, (iii) 75%, and (iv) 1 (t_f is the final time).

properties of a similar nickel-based superalloy, IN718 [34], were used. Effective thermal conductivity for superalloy powder of fully dense material at a temperature of 1150 °C is 28.75 W/m K, and thermal conductivity of stainless steel container at a temperature of 1150 °C is 22 W/m K.

Heat loss due to air convention during transport was ignored due to the short transfer time. Since the initial temperature of the container and the powder were the same, it was assumed that no heat transfer occurred between them. In this coupled thermo-mechanical process, heat transfer coefficient between the H13 die and stainless steel container was 20 kW/m^2 K [35]. The friction between the powder and the inner wall of the dies, and between the outer surface of the container and the H13 dies were assumed as 0.3 [36].

5. FE model results

5.1. FE model verification

In order to validate the FE model, the measured and simulated results of the load variation with stroke and the relative density distribution have been compared. Fig. 6 shows the load variation with stroke during direct powder forging, obtained from the oscilloscope record and FE result. The load is increased gradually with the increasing stroke. The maximum load is 220 kN. The load and stroke variation are in good agreement with the experimental result: the maximum error between the predicted and measured value is 18%. The error could be due to the fact that the friction coefficient defined in the FE model is a rough value; in addition, the air convenction during transferring from the furnace to the die-set is ignored in the FE simulation.

Fig. 7 shows the relative density distribution after deformation, obtained from experiment and FE simulation. Twenty points along the horizontal centre line were selected for the FE results, and the relative density at each point is shown in Fig. 7. The predicted relative densities are in a good agreement with the measured ones.

The close match of predicted relative density with practical experimental result provides reasonable validation of the FE model. Therefore, it is assumed that the FE model developed in this paper can be used to predict the relative density distribution of the direct powder forging process.

5.2. Prediction of in-process variables

The principle aim of the powder forging is pore closure as well as particle bonding. This is critically dependant on the stress state during hot forging [11]. Fig. 8 shows the distribution of effective stress and mean stress at different times. As shown in Fig. 8(a), at time equals 25%, 50% and 75% of the total time (t_f), since friction exists between the test-piece and the tools, the effective stress is decreased when the location is away from the centre. When time equals t_f, the effective stress in the centre is lower than that at location P2, P3 and P4, which is attributed to the adiabatic heating. The temperature in the centre is higher than that at other locations due to larger plastic deformation, and thus the effective stress is lower. Fig. 8(b) shows the distribution of the mean stress, which is the average of the three principal stresses. A negative value of mean stress indicating the compressive deformation is beneficial to volume shrinking and thus pore closure. At the centre of the test-piece, the mean stress is a negative value for all of the time. At the edge of the test-piece, i.e. P5, the mean stress is positive before time equals 75% of t_f. When time equals t_f, the mean stress at the edge becomes negative.

Stress triaxiality is defined as the ratio of mean stress to the effective stress. Many works have demonstrated that it is one of the key aspects affecting void coalescence in porous materials [37,38]. When the hydrostatic stress is compressive, the stress triaxiality becomes negative; therefore porosity closure will be promoted. Fig. 9 shows the variations of stress triaxiality, effective strain and relative density with time at five different locations. The stress triaxiliaty at locations P1, P2, P3 and P4 are negative, indicating that the compressive deformation takes place. The effective strain is decreased from the centre to the edge due to friction. At the location of P5, i.e. the edge of the test-piece, the effective strain is less than 0.2. With an increasing time, relative densities at these locations are increased at different rate, which has the correlation with the effective strain and triaxiality: a smaller negative value of triaxiality and a larger effective strain can prompt the porosity elimination with a higher rate. When time equals 50% of t_f, the triaxiality of P1 and P2 are similar, but the effective strain of P1 is larger than that of P2; therefore the relative density of P1 is larger than that of P2. The triaxiality of P5 is positive until time equals 94% of t_f, and then is negative, and thus the relative density of P5 has little variation before time equals 94% of t_f, and a small increase after 94% of t_f.

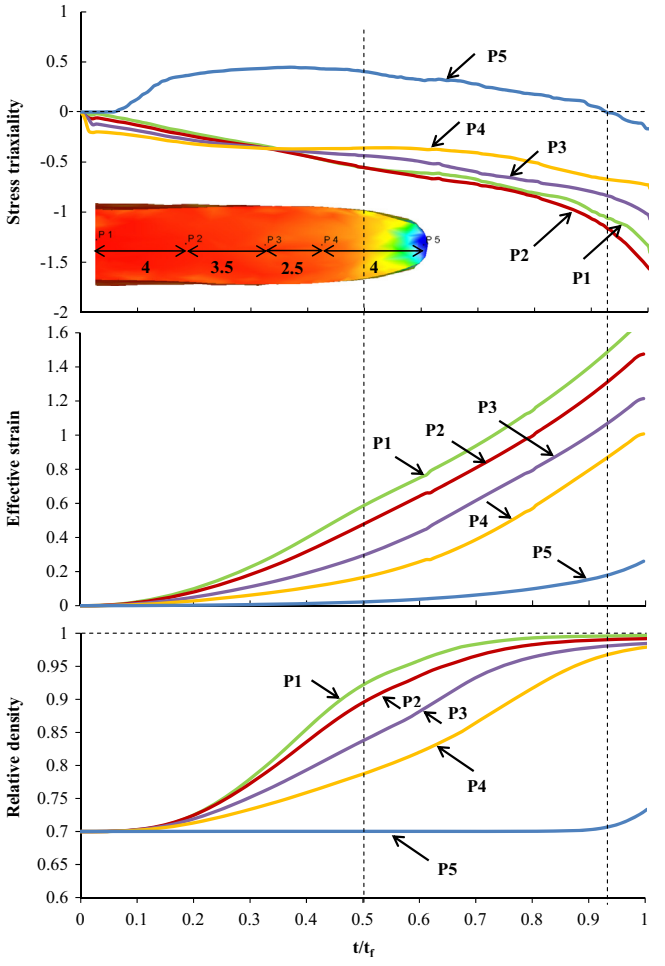

Fig. 9. Stress triaxiality, effective strain and relative density with time at different locations (mm) (t_f is the final time).

6. Conclusions

A new net-shape forging process has been proposed for processing powder superalloys, at low cost and with high productivity. Experimental compression tests have been conducted on encapsulated nickel-based superalloy. Microstructure and consolidation condition

have been obtained by SEM observation. Within a distance of 10 mm from the centre of the formed test-piece, the relative density reached 1.0. The distribution of PPBs is isolated and dispersed. FE simulations have been carried out in DEFORM to analyse the stress state during forming. The correlation between the stress triaxiality, effective strain and consolidation condition has been rationalised. It is concluded that with sufficient compressive stress, the powder can be fully consolidated. The FE model developed here can be used to predict the stress state and thus to predict the relative density; therefore the geometry and the thickness of the container can be optimised for a certain component, which provides a guide to design the direct forging preform.

Acknowledgements

Much appreciated is the strong support received from the Beijing Institute of Aeronautical Materials (BIAM), for this funded research. The research was performed at the AVIC Centre for Materials Characterisation, Processing and Modelling at Imperial College London (Grant No: MESM P42745).

References

[1] B. Williams, International Powder Metallurgy Directory, 15th Edition, 2012-2013, 2012.
[2] G. Raisson, J.Y. Guédou, D. Guichard, J.M. Rongvaux, Adv. Mater. Res. 278 (2011) 277–282.
[3] M.O. Alniak, F. Bedir, Mater. Sci. Eng.: B 130 (2006) 254–263.
[4] S.L. Semiatin, K.E. McClary, A.D. Rollett, C.G. Roberts, E.J. Payton, F. Zhang, T.P. Gabb, Metall. Mater. Trans. A 44 (2013) 2778–2798.
[5] R.J. Mitchell, J.A. Lemsky, R. Ramanathan, H.Y. Li, K.M. Perkins, L.D. Connor, Superalloys, TMS, Pennsylvania, USA (2008) 347–356.
[6] A.S. Helle, K.E. Easterling, M.F. Ashby, Acta Metall. 33 (1985) 2163–2174.
[7] E. Arzt, M.F. Ashby, K.E. Easterling, Metall. Trans. A 14 (1983) 211–221.
[8] C. Bampton, W. Goodin, T.V. Daam, G. Creeger, S. James, Proceedings of International Conference on Hot Isostatic Pressing, 2005.
[9] C. Qiu, Department of Metallurgy and Materials, The University of Birmingham, Birmingham, 2010.
[10] H.A. Kuhn, in: PeterW. Lee, Yves Trudel, Ronald Iacocca, et al., (Eds.), Forging and hot pressing, shaping and consolidation technologies, Powder Metal Technologies and Applications, vol. 7, ASM International, Ohio, United States, 1998.
[11] R.J. Dashwood, G.B. Schaffer, Mater. Sci. Eng.: A 323 (2002) 206–212.
[12] R.E.D. Mann, R.L. Hexemer Jr, I.W. Donaldson, D.P. Bishop, Mater. Sci. Eng.: A 528 (2011) 5476–5483.
[13] R.W. Cooke, G. Steedman, D.P. Bishop, R.L. Hexemer Jr., I.W. Donaldson, International Conference on Powder Metallurgy and Particulate Materials, Chicago, United States, 2013, pp. 3108–3119.
[14] J. Das, K. Chandra, P.S. Misra, B. Sarma, Mater. Sci. Eng.: A 479 (2008) 164–170.
[15] W.J. Rozmus, US Patent 4142888, 1979.
[16] G.D. Pfaffmann, US Patent 4704252, 1987.
[17] H.S. Meeks, M.S. Fleming, US 6630008, 2003.
[18] J.J. Conway, F.J. Rizzo, Hot isostatic pressing of metal powders, shaping and consolidation technologies, Powder Metal Technologies and Applications, vol. 7, ASM International, 1998.
[19] D.P. DeLo, H.R. Piehler, Acta Mater. 47 (1999) 2841–2852.
[20] Y. Zhou, S. Rao, Z. Zhang, Z. Zhao, Mater. Des. 49 (2013) 25–27.
[21] M.T. Kim, O.Y. Oh, J. Alloy. Compd. 477 (2009) 224–232.
[22] G.H. Gessinger, Powder Metallurgy of Superalloys, Butterworths, London, 1984.
[23] L. Zhang, H. Liu, X. He, d. Rafi ud, X. Qu, M. Qin, Z. Li, G. Zhang, Mater. Charact. 67 (2012) 52–64.
[24] A.M. Wusatowska-Sarnek, M.J. Blackburn, M. Aindow, Mater. Sci. Eng.: A 360 (2003) 390–395.
[25] H.V. Atkinson, S. Davies, Metall. Mater. Trans. A 31 (2000) 2981–3000.
[26] E.A. Olevsky, Mater. Sci. Eng.: R: Rep. 23 (1998) 41–100.
[27] M. Abouaf, J.L. Chenot, G. Raisson, P. Bauduin, Int. J. Numer. Methods Eng. 25 (1988) 191–212.
[28] S. Shima, M. Oyane, Int. J. Mech. Sci. 18 (1976) 285–291.
[29] S.M. Doraivelu, H.L. Gegel, J.S. Gunasekera, J.C. Malas, J.T. Morgan, J.F. Thomas Jr, Int. J. Mech. Sci. 26 (1984) 527–535.
[30] DEFORM v11.0 Documentation, Scientific Forming Technologies Corporation, Columbus, Ohio, 2014.
[31] J. Lin, Y. Liu, J. Mater. Process. Technol. 143 (2003) 281–285.
[32] H. Li, J. Lin, T.A. Dean, S.W. Wen, A.C. Bannister, Int. J. Plast. 25 (2009) 1049–1065.
[33] R.H. Bogaard, P.D. Desai, H.H. Li, C.Y. Ho, Thermochim. Acta 218 (1993) 373–393.
[34] Y.P. Lin, Mechanical Engineering, University of Birmingham, Birmingham, UK, 2010.
[35] P. Dadras, W.R. Wells, J. Manuf. Sci. Eng. 106 (1984) 187–195.
[36] Y.S. Na, J.T. Yeom, N.K. Park, J.Y. Lee, J. Mater. Process. Technol. 141 (2003) 337–342.
[37] Y. Zhang, Z. Chen, Int. J. Fract. 143 (2007) 105–112.
[38] G. Vadillo, J. Fernández-Sáez, Eur. J. Mech. – A/Solids 28 (2009) 417–427.